Quantitative Determination of Loss Properties of Semiconductor Laser Beams Propagating in Hollow Waveguides

Liming Yuan, Shuo Meng, Jin Liu, Kebin Tong, Jinyi Li, Shuanke Wang, and Zhenhui Du

***Abstract*—The loss properties of semiconductor laser beams propagating in hollow waveguides (HWGs) are crucial in several applications. The attenuation coefficient of the distributed feedback quantum cascade laser (DFB-QCL) in the HWG was quantitatively determined by measuring its beam profile and laser power along the length of the HWG. The experimental reliability was evaluated, with measurement uncertainties as low as 2.6% and 0.5% for the full width at half maximum (FWHM) of beam profile and the laser power, respectively. We derived an empirical formula for the attenuation coefficient, which is exponential rather than linear with the length of the HWG. The formula was verified to be highly accurate, with a 76.2% reduction in deviation compared to the data in the datasheet. We propose a new concept for a free optical path (FOP) that depends on the inner diameter of the HWG and the incident angle of the beam. The FOP could be an excellent parameter for designing or optimizing HWG-based sensors.**

***Index Terms*—Hollow waveguide, semiconductor laser beam, propagation properties, attenuation coefficient.**

I. Introduction

HOLLOW waveguides (HWGs) in the form of hollow capillary tubes with metal/dielectric internal coatings are promising for transmitting laser beams owing to their advantages of flexibility, high-power threshold, low transmission loss, absence of end reflections, and broadband ranging from X-rays to ultraviolet, visible, infrared (IR), and terahertz radiation [1]–[6]. These advantages offer a broad scope for developing HWG applications, such as laser power delivery in laser surgery [7], IR thermal image sensing for disease diagnosis [8], [9], and trace gas detection for breath analysis and environmental monitoring [10]–[15]. However, the system performance and integration scale of photonic devices employing HWGs rely on knowledge and accurate and precise transmission parameters with a specific laser source.

Manuscript received March 2, 2022; accepted March 19, 2022. Date of publication March 28, 2022; date of current version April 11, 2022. *(Corresponding author: Zhenhui Du.)*

Liming Yuan, Shuo Meng, Jin Liu, Kebin Tong, Shuanke Wang, and Zhenhui Du are with the State Key Laboratory of Precision Measuring Technology and Instruments, Tianjin University, Tianjin 300072, China (e-mail: yuanliming@tju.edu.cn; mengsh@tju.edu.cn; liu_jin@tju.edu.cn; tongkebin@tju.edu.cn; wangshuanke@tju.edu.cn; duzhenhui@tju.edu.cn).

Jinyi Li is with the Key Laboratory of Advanced Electrical Engineering and Energy Technology, Tiangong University, Tianjin 300387, China (e-mail: lijinyi@tiangong.edu.cn).

Digital Object Identifier 10.1109/JPHOT.2022.3161615

The propagation properties of laser beams in HWGs have received considerable attention [16]–[21]. Many studies have focused on theoretical models for light transmission in metallic and dielectric waveguides, and have provided explanations of laser modes and energy loss on average [22], [23]. Recently, much attention has been paid to HWG-based compact sensors combined with quantum cascade lasers (QCLs) or interband cascade lasers (ICLs) [24]–[26]. These lasers present distinctive features of single-mode, Gaussian beams and high angular spread [27]–[29], which lead to different propagation properties in HWGs.

Patimisco *et al.* [30] compared the average attenuation coefficients of an external-cavity QCL beam propagating in HWGs coated with Ag/AgI, Ag/Ps and Ag/AgI/Ps. Their results showed that the Ag/Ps-coated HWG had the lowest attenuation coefficient of 0.44 dB/m. They also investigated the coupling conditions optimizing and output beam quality with the influence of bore diameter and HWG length by using an IR camera and four QCLs of 3.7∼7.6 μm [31]. Based on IR imaging method, Sampaolo *et al.* [32] demonstrated the QCL beam single mode propagation through Ag/AgI-coated HWGs with a bore size of 200 μm in the spectral range of 5.1∼10.5 μm, and measured the transmission loss at different coupling conditions by changing the coupling lens. Francis *et al.* [33] coupled a 7.8 μm pulsed QCL with Ag/AgI-coated HWGs and verified that a thermal imaging camera could obtain more detailed images of the output intensity distributions from the HWGs. However, the loss of laser transmission by an HWG typically decreases as the transmission distance increases, particularly for a laser beam with a large angle, owing to the gradual reduction in the leakage of the laser power into the cladding of the HWG. Therefore, the average attenuation coefficients of HWGs calculated according to the method in the literature [30]–[32] or provided in standard specifications cannot be used as a basis for accurately designing and developing applications involving laser-HWG systems.

In this study, we characterized the propagation properties of Ag/AgI-coated HWGs coupled with a continuous-wave QCL via IR imaging and by fitting the beam profile and laser power at various lengths along the HWG. Furthermore, we derived an empirical formula to calculate the attenuation coefficient of a semiconductor laser beam propagating in an Ag/AgI-coated HWG.

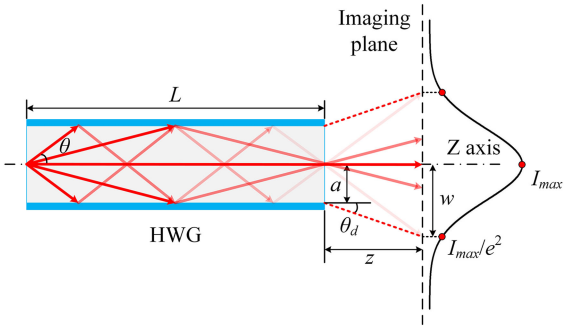

Fig. 1. Ray model describing laser beam propagation in an HWG.

II. Theoretical Calculation

The laser power P in an HWG with length L is assumed to be $P(L)$. The transmission loss A of an HWG can be calculated from the ratio between the power at the waveguide entrance and that measured at the waveguide exit [30]:

$$A(L) = 10\log[P(0)/P(L)] = P_{abs}(0) - P_{abs}(L) \quad (1)$$

where P_{abs} is the absolute value of P, which is calculated by

$$P_{abs}(L) = 10\log[P(L)/1mW] \quad (2)$$

Therefore, the relationship between attenuation coefficients α and L can be obtained by performing a derivative operation in Eq. (1).

$$\alpha(L) = dA/dL = -P_{abs}'(L) \quad (3)$$

The precise description of the loss must be consistent with the intensity distribution. The transverse profile of the optical intensity I of a beam with power P can be described using a Gaussian function as follows:

$$I(r) = \frac{P}{\pi w^2/2}\exp\left(-2\frac{r^2}{w^2}\right) \quad (4)$$

where r denotes the distance from the beam axis and w denotes the beam radius, which is defined as the distance from the beam axis where the intensity drops to $1/e^2$ of the maximum value.

A Gaussian beam can be decomposed into a myriad of rays or plane waves that are coupled to the HWG at different angles and transmitted according to well-established principles of geometrical optics (Fig. 1). Because the value of A depends on the interaction between the laser beam and the inner wall of the HWG during reflection, A increases as the divergence angle θ_d of the beam propagating in the HWG increases owing to an increase in the number of reflections occurring throughout the length of the HWG. Therefore, A is related to θ_d. Furthermore, w is a function of L and is denoted by $w(L)$. Then, θ_d can be calculated as:

$$\theta_d(L) = \arctan\{[w(L) - a]/z\} \quad (5)$$

where z is the vertical distance along the beam axis from the waveguide exit to the imaging plane, and a denotes the inner radius of the HWG.

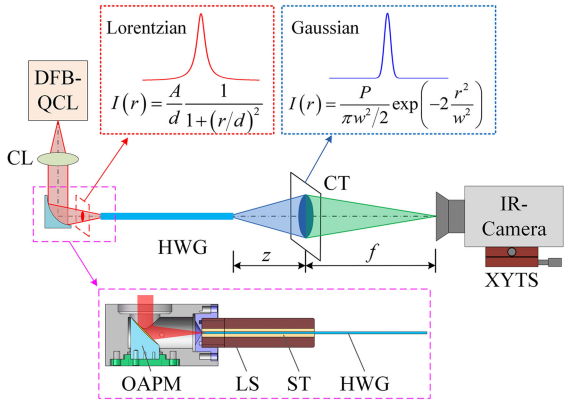

Fig. 2. Schematic of the experimental setup using straight HWGs of various lengths. The profiles of the incident and near-field emitted laser beam and the corresponding fitting formulas were shown in the red- and blue-outlined panels, respectively. The purple-outlined panel showed the self-made coupling component. DFB-QCL: distributed feedback quantum cascade laser, CL: collimating lens, OAPM: off-axis parabolic mirror, LS: limit sleeve, ST: silicone tube, CT: cardboard target, XYTS: XY translation stage.

Consequently, the relationship between α and θ_d can be established by combining Eqs. (3) and (5):

$$\alpha(\theta_d) = \varphi(\theta_d) \quad (6)$$

III. Experiments

A. Experimental Setup

The experimental setup employed in this study is illustrated in Fig. 2. A distributed feedback quantum cascade laser (DFB-QCL) (QD7950CM1, Thorlabs, Inc., USA) operating at $\lambda = 8.004\ \mu$m was used as the laser source. The DFB-QCL was installed on a commercial laser mount with an aspheric lens (C036TME-F; Thorlabs, Inc.; $f = 4.0$ mm). The collimated laser was coupled with HWGs using a self-made coupling component, which comprised an off-axis parabolic mirror (MPD127127-90-M01, Thorlabs, Inc.; $f = 25.4$ mm) to focus the laser, a metal sleeve to limit the position of HWGs and a silicone tube to fix HWGs. This design ensured that the entrance of the straight Ag/AgI-coated HWG (HWEA10001600, Polymicro Technologies, USA) with a 1000 μm bore was located at the beam waist of the incident laser, and the size of the beam waist was smaller than the inner diameter of the HWG, even when the HWG was replaced. The cross-section of the transmitted laser beam in the XY plane was collected at a cardboard target using an IR camera (ThermoVision A40, FLIR Systems, Inc., USA) with a pixel size of 0.224 mm, which was mounted on a compact motorized XY translation stage. The cardboard target was placed at the focal length of the IR camera (i.e., $f = 400$ mm) to attenuate a part of the laser energy to protect the detector of the IR camera from being damaged. The vertical distance between the cardboard target and the waveguide exit was 6.5 mm. The total output power of the HWG was measured using an optical power meter (OPM) (Vega-12A, Ophir Optronics, LLC, USA) located 5 mm from the waveguide exit.

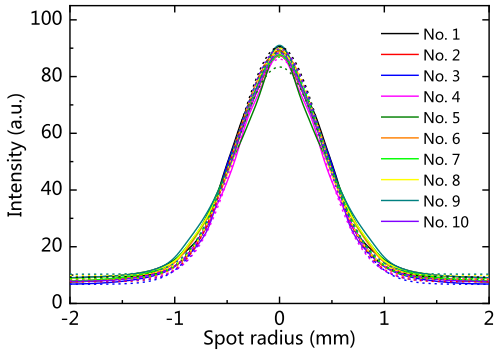

Fig. 3. Experimental laser beam profiles: raw experimental data (solid lines) and curves fitted based on the membership function-weighted Levenberg–Marquardt (MFW-LM) algorithm [34] (dashed lines).

TABLE I
RELATIVE ERROR, INTEGRAL AREA, FULL WIDTH AT HALF MAXIMUM, AND TOTAL OUTPUT OPTICAL POWER VALUES

Exp. No.	δ [%]	*Area* [a.u.]	FWHM [mm]	P_{out} [mW]
1	1.46	82.95	0.96	44.3
2	0.61	84.14	0.97	44.5
3	0.47	86.38	0.99	44.4
4	1.26	76.57	0.93	44.7
5	2.23	80.84	1.01	44.8
6	0.25	82.94	0.98	44.9
7	0.65	82.32	0.99	44.6
8	1.25	79.52	0.95	44.6
9	1.65	80.27	0.96	44.3
10	0.09	82.09	0.94	44.7
RSD [%]	-	3.3	2.6	0.5

Exp. No.: experiment number
δ: repeated experiments relative error
Area: integral area
FWHM: full width at half maximum
P_{out}: total output optical power

B. Performance Evaluation of the Experimental System

We verified the stability and measurement repeatability of the experimental system by conducting ten experiments under equivalent experimental conditions, while following the same experimental and data processing procedures. Fig. 3 shows the experimental one-dimensional emitted laser beam profiles and the results obtained by fitting the experimental data based on the membership function-weighted Levenberg–Marquardt (MFW-LM) algorithm. The MFW-LM algorithm uses the membership function as the weighting function of fitting for signal modeling and reconstruction under the expected mathematical model constraints, as detailed in our previous work [34]. The statistical results for the integral area (*Area*) and full width at half maximum (FWHM) of the fitted laser beam profiles are listed in Table I. A standard laser beam profile curve was obtained from the average of the ten fitted profile curves, and the relative error δ of the repeated experiments (i.e., the deviation between the fitted profile curves and the standard profile curve) was expressed by the relative mean square root of the fitting residual as follows:

$$\delta = \sqrt{\sum_{i=1}^{N} \left[(y_i - y_i^*)/y_{\max}\right]^2 \Big/ N} \tag{7}$$

where y_i and y_i* denote the fitted data value and standard value, respectively; $y_{\max}$ is the maximum value among all y_i; and N denotes the number of fitted points. The values of δ for the ten experiments are listed in Table I.

In addition, the relative standard deviation (RSD) was used to represent the stability errors for the key parameters of the laser beam profile (i.e., *Area* and FWHM):

$$RSD = \sqrt{\sum_{i=1}^{N} (v_i - \overline{v})^2} \Big/ \left(\overline{v}\sqrt{n-1}\right) \times 100\% \tag{8}$$

where v_i and $\bar{v}$ denote the measured and average values, respectively, and n denotes the number of repeated experiments. The RSD values of *Area* and FWHM were only 3.3% and 2.6%, respectively.

The measured results of ten repeated experiments obtained from the OPM for the output optical power (P_{out}) emitted from a straight HWG of length 0.196 m are shown in the last column of Table I. The RSD of P_{out} was as low as 0.5%, indicating that our experiments exhibited excellent coupling repeatability and reliability.

The deviations of *Area* and FWHM are mainly caused by the resolution of the IR camera (0.224 mm) and the fitting error of the MFW-LM algorithm. And the deviation of P_{out} is mainly caused by the measurement accuracy of the OPM and the influence of ambient light.

IV. Results and Discussion

A. Attenuation Coefficient Along the Waveguide Length

The attenuation coefficient of the HWG was investigated by measuring the optical output power at the exit of the HWG of various lengths under the same incident conditions. There were ten lengths of HWGs, 0.137 m, 0.196 m, 0.302 m, 0.432 m, 0.593 m, 0.719 m, 0.840 m, 1.037 m, 1.651 m, and 2.032 m, for the measurements. The recorded optical power (mW) emitted from these HWGs is shown in Fig. 4(a). The maximum deviations of the optical power for various lengths are less than 0.5% of the corresponding measured value. Considering the customary unit of the decibel, we transformed the unit of recorded power from mW to dBm, as shown in Fig. 4(b). The emitted laser power exhibited an obvious nonlinear relationship with the HWG length. This relationship was identified to be exponential by further investigation. The results were fitted using an exponential function, as shown in Fig. 4(a) and (b). They showed that the fittings were very good, with an R-square of 1 and a very low residual of 0.01%.

We calculated the attenuation coefficient of the HWG by differentiating the fitted formula of the laser power with the HWG length in Fig. 4(b), as shown in Fig. 4(c). The attenuation coefficient with respect to HWG length is expressed as

$$\alpha(L) = 5.801e^{-1.324L} \tag{9}$$

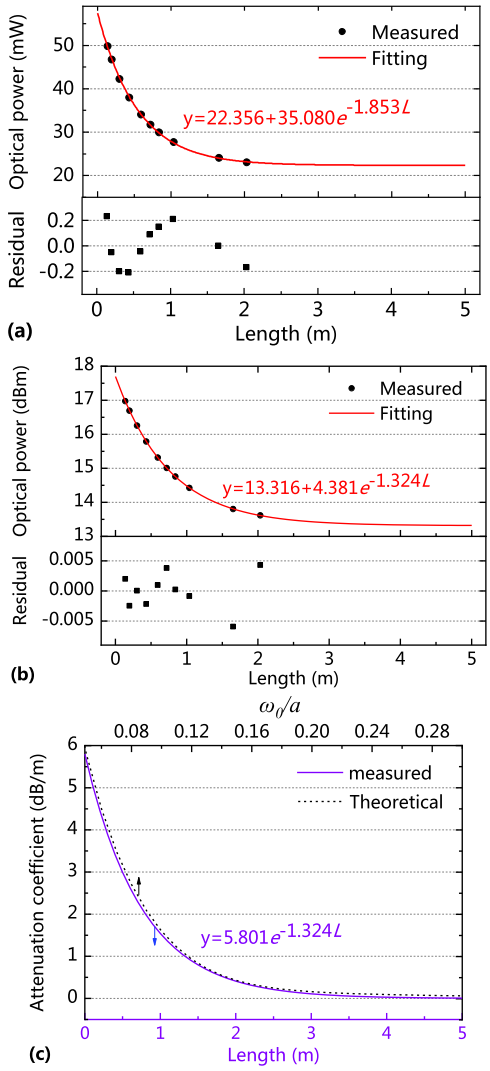

Fig. 4. Measured output optical power of HWGs with various lengths in units of (a) mW and (b) dBm, and (c) attenuation coefficient calculated from fitting experimental data.

The results exhibited an exponential attenuation coefficient with the HWG length; that is, the loss coefficient decreased along the HWG length. This differs from the HWG datasheet used in the test. The relationship between the attenuation coefficient and HWG length is reminiscent of the theoretical loss coefficient obtained using the mode model [32], [35]. The measured attenuation coefficient was compared with the theoretical loss coefficient, as shown in Fig. 4(c). The theoretical loss coefficient was plotted against the upper horizontal axis of the ratio ω_0/a, where ω_0 is the laser beam waist. They showed amazing consistency.

The loss of an HWG of any length can be precisely calculated using Eq. (9). The calculated loss for a 0.5 m-long HWG based on the average attenuation coefficient of 1 dB/m provided in the datasheet was 0.5 dB, while that according to Eq. (9) is 2.1 dB. Therefore, using Eq. (9) reduces the error in the calculation of the loss by 76.2% relative to the loss obtained from the HWG datasheet.

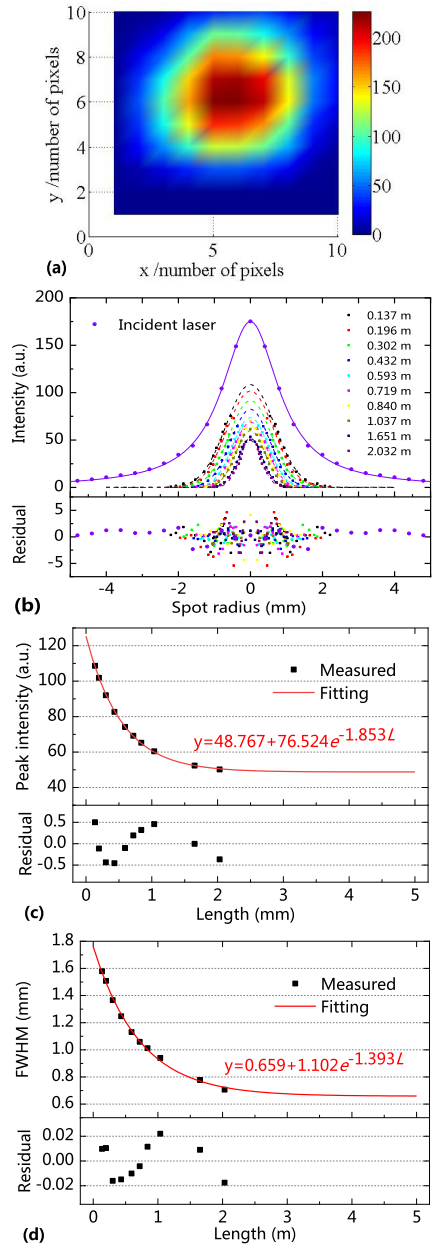

Fig. 5. Measured results of the laser beam: (a) two-dimensional image of the laser beam emitted from the DFB-QCL obtained by using an IR camera, and (b) reconstructed laser beam profiles (solid lines) emitted from the DFB-QCL (incident laser) and straight HWGs with various lengths using Lorentzian and Gaussian functions, respectively, based on the MFW-LM algorithm, and (c) relationship between the peak intensity and the HWG length, and (d) relationship between the FWHM and the HWG length.

B. Laser Beam Profile Properties

We measured the laser beam profiles before and after propagation in straight HWGs of various lengths using an IR camera to address the relationship between the attenuation coefficient and divergence angle. A two-dimensional image of the laser beam emitted from the DFB-QCL, that is, the incident laser beam, is shown in Fig. 5(a). The laser intensity is indicated by the color scale in the figure. We calculated the average intensity

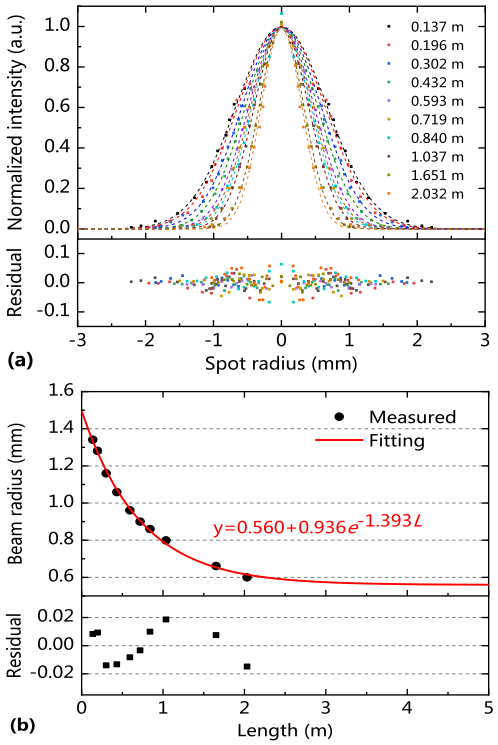

Fig. 6. Characteristic analysis results of the laser beam: (a) normalized laser beam profiles emitted from straight HWGs with various lengths, and (b) relationship between the beam radius and the HWG length.

distributions of the incident and output laser beams along the radial direction and then reconstructed them using Lorentzian and Gaussian functions, respectively, based on the MFW-LM algorithm, as shown in Fig. 5(b). Obviously, the incident laser beam has a typical Lorentzian profile, which is determined by the structural characteristics of the single-mode semiconductor laser [27], [28]. However, even if the HWG length was very short (0.137 m), the laser beam emitted from the HWG exhibited a typical Gaussian profile. This is because the laser beam evolved from a Lorentzian beam to a Gaussian beam under the loss effect of the HWG [29].

We extracted the peak intensity of the laser beam profiles with various HWG lengths in Fig. 5(b), and then did an exponential fit, as shown in Fig. 5(c). The fitting results show that the rate of the reduction of the peak intensity in terms of the distance is -1.853, which is expectedly equal to the rate of the reduction of the optical power in terms of the HWG length in Fig. 4(a). Moreover, we also extracted the FWHM of the laser beam profiles with various HWG lengths in Fig. 5(b), as shown in Fig. 5(d). The exponential fitting results show that the rate of the reduction of the FWHM in terms of the HWG length is -1.393.

We normalized the maximum intensity of the reconstructed laser beam profiles emitted from straight HWGs of various lengths to 1 (arbitrary unit) to investigate the variation law of beam radius, as shown in Fig. 6(a). The beam radius of the Gaussian profiles decreases rapidly as the length increases, indicating that components with larger divergence angles in the laser beam suffer greater losses until they are completely lost. The

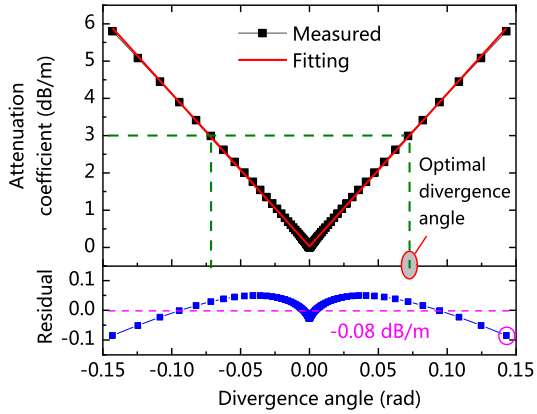

Fig. 7. Relationship between attenuation coefficient and divergence angle.

values of the beam radius were extracted from the reconstructed Gaussian profiles and fitted to an exponential function, as shown in Fig. 6(b). The rate of the reduction of the beam radius in terms of the HWG length in Fig. 6(b) is reasonably equal to the rate of the reduction of the FWHM in terms of the HWG length in Fig. 5(d). The beam radius with respect to the HWG length is expressed as

$$w\left(L\right) = 0.560 + 0.936e^{-1.393L} \tag{10}$$

From the fitting results, the following conclusions can be drawn. When a laser with a larger beam radius propagates in an HWG, the value of the beam radius decreases exponentially with an increase in the transmission distance because the loss of laser energy far from the beam axis in the HWG is greater. When the beam radius is reduced to a value close to the inner radius of the HWG, the loss tends to zero and the value of the beam radius remains constant.

Note that, the reduction in the FWHM with an increase in the HWG length extracted from Fig. 6(a) is the same as that extracted from Fig. 5(b), as shown in Fig. 5(d). Because Fig. 6(a) is only the result of the normalization of the maximum intensity of Fig. 5(b). And the normalization operation does not change the FWHM.

C. Influence of Divergence Angle on Attenuation Coefficient

We investigated the attenuation coefficient with various divergence angles θ_d by combining Eq. (5), (9), and (10), as shown in Fig. 7(black rectangular lines). The attenuation coefficient exhibited an obvious linear relationship with the divergence angle. A linear fit of the data was performed, and the maximum residual was as low as 0.08 dB/m. The corresponding expression of the attenuation coefficient with respect to the divergence angle is given by:

$$\alpha\left(\theta_d\right) = 0.030 + 40.941\theta_d \tag{11}$$

The fitting results (red line in Fig. 7) show that the attenuation coefficient increased linearly with the divergence angle. This is because a Gaussian beam transmission with a relatively larger

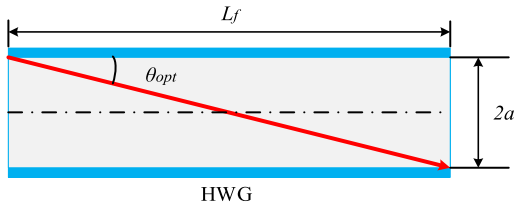

Fig. 8. Schematic of the free optical path.

divergence angle undergoes a greater number of reflections and accordingly suffers a higher loss. Within a certain length range, the number of reflections has a linear relationship with divergence angle. Therefore, using a Gaussian beam with a smaller divergence angle as the light source for an HWG can effectively reduce the loss of laser energy.

In addition, for a semiconductor laser with a short cavity, a tradeoff exists between coupling efficiency and transmission efficiency. Here, the long focal length required to ensure a small divergence angle increases the beam waist and reduces coupling efficiency. Conversely, the high coupling efficiency of a short focal length will eventually be offset by the high HWG attenuation.

D. Free Optical Path

The divergence angle of the incident laser is the most commonly used parameter in the design and application of HWG-based sensors. We defined the angle between the HWG optical axis and the laser beam at an attenuation coefficient of 3 dB/m as the optimal divergence angle θ_{opt} required to ensure excellent transmission performance. Furthermore, we propose the concept of a free optical path (FOP) L_f, which is defined as the ratio of the inner diameter of an HWG to the tangent of the optimal divergence angle (Fig. 8) and is given by

$$L_f = 2a/\tan\left(\theta_{opt}\right) \tag{12}$$

The physical meaning of FOP is the waveguide length when the attenuation coefficient is 3 dB/m.

The relationship between the attenuation coefficient and waveguide length for a 1000 μm bore Ag/AgI-coated HWG can be changed from Eq. (9) to

$$\alpha\left(L\right) = 5.801e^{-0.018L/L_f} \tag{13}$$

Accordingly, a longer FOP can result in a lower loss for the HWGs. When the inner diameter decreases, the FOP becomes shorter, and thus the number of reflections per unit length of the HWG increases, resulting in an increase in loss, and vice versa. Moreover, for the same HWG, the FOP when placed in a bend is shorter than that in a straight one. Furthermore, the smaller the bending radius, the shorter the FOP. Essentially, the bending of the HWG causes the incident angle of the light to the inner wall to increase, and the number of reflections per unit length to increase, thereby increasing the loss. However, the loss in HWGs is highly dependent on the launch conditions [35].

The FOP parameter can also be used to design the structure of HWG-based sensors. One of the key processes in HWG-based sensor design is to determine the laser power and signal-to-noise ratio (SNR) of the signal channel, which can be achieved by accurately calculating the transmission loss in the HWG using Eq. (13). The length of the HWG and the absorbance can be determined by the absorption coefficient of the target gas and the required detection limit, and the sensor structure can be determined accordingly. For example, in trace gas detection applications, the loss can be reduced by selecting an HWG with a large inner diameter and a straight or large bending radius arrangement, thereby improving the system SNR and reducing the system detection limit.

V. Conclusion

In summary, we characterized and quantitatively determined loss properties of HWGs by investigating the QCL beam profile and laser power before and after propagation in HWGs at various lengths. The obtained attenuation description is particularly suitable for single-mode semiconductor lasers with Lorentzian beams, where mode analysis is no longer applicable. By investigating the laser power at different positions along the HWG length, we found that the attenuation coefficient was not constant, as described in the HWG datasheet, but had an exponential relationship with the length. We derived and verified a new model that indicated that the attenuation coefficient increased linearly with an increase in the divergence angle. The deviation of the new model from the measured value was as low as 0.08 dB/m. In addition, we propose the concept of an FOP that can be used to design or optimize low-loss HWG-based sensors. The method provides strong support for improving the system performance and integration scale of photonic devices using HWGs.

References

[1] J. A. Harrington, "A review of IR transmitting, hollow waveguides," *Fiber Integr. Opt.*, vol. 19, no. 3, pp. 211–227, 2000.
[2] O. Kfir *et al.*, "Generation of bright phase-matched circularly-polarized extreme ultraviolet high harmonics," *Nat. Photon.*, vol. 9, no. 2, pp. 99–105, 2015.
[3] J. E. Melzer and J. A. Harrington, "Investigation of silver-only and silver/TOPAS (R) coated hollow glass waveguides for visible and NIR laser delivery," *Opt. Fibers Sensors for Med. Diagnostics Treat. Appl. XV*, vol. 9317, 2015, Art. no. 93170H-1-9.
[4] Y. Milstein *et al.*, "Photothermal imaging bundle system for estimating tissue oxygen saturation," *Opt. Fibers Sensors for Med. Diagnostics Treat. Appl. XII*, vol. 8218, 2012, Art. no. 82180D-1-7.
[5] M. Navarro-Cía *et al.*, "Silver-coated teflon tubes for waveguiding at 1-2 THz," *J. Infrared Milli. Terahz. Waves*, vol. 36, no. 6, pp. 542–555, 2015.
[6] C. D. Rabii and J. A. Harrington, "Mechanical properties of hollow glass waveguides," *Opt. Eng.*, vol. 38, no. 9, pp. 1490–1499, 1999.
[7] C. Jing, W. Kendall, and J. A. Harrington, "A simple way to establish a dual-core hollow fiber for laser surgery applications," *Opt. Fibers Sensors for Med. Diagnostics Treat. Appl. XVI*, vol. 9702, 2016, Art. no. 97020D-1-10.
[8] B. Dekel *et al.*, "Fiber optic thermal imaging system based on hollow glass waveguides or silver halide fibers as scanning elements," *Opt. Eng.*, vol. 39, no. 4, pp. 941–946, 2000.
[9] U. Gal *et al.*, "Coherent hollow-core waveguide bundles for thermal imaging," *Appl. Opt.*, vol. 49, no. 25, pp. 4700–4709, 2010.
[10] J. Wei *et al.*, "Miniaturization of hollow waveguide cell for spectroscopic gas sensing," *Sens. Actuator B*, vol. 243, pp. 254–261, 2017.

[11] L. Liu, B. Xiong, Y. Yan, J. Li, and Z. Du, "Hollow waveguide-enhanced mid-infrared sensor for real-time exhaled methane detection," *IEEE Photon. Technol. Lett.*, vol. 28, no. 15, pp. 1613–1616, Aug. 2016.
[12] J. Li *et al.*, "Quantitative analysis of ammonia adsorption in Ag/AgI-coated hollow waveguide by mid-infrared laser absorption spectroscopy," *Opt. Lasers Eng.*, vol. 121, pp. 80–86, 2019.
[13] J. Li *et al.*, "Hollow waveguide enhanced dimethyl sulfide sensor based on a 3.3 μm interband cascade laser," *Sens. Actuator B*, vol. 255, pp. 3550–3557, 2018.
[14] J. Li *et al.*, "Applications of hollow waveguide in spectroscopic gas sensing," *Spectrosc. Spectral Anal.*, vol. 37, no. 7, pp. 2259–2266, 2017.
[15] Z. Du *et al.*, "Towards high-precision hollow waveguide-based gas sensors adapting nonuniform pressure and immune to flow fluctuation," *Sens. Actuator B*, vol. 308, 2020, Art. no. 127703-1-6.
[16] E. A. J. Marcatili and R. A. Schmeltzer, "Hollow metallic and dielectric waveguides for long distance optical transmission and lasers," *Bell Syst. Tech. J.*, vol. 43, no. 4, pp. 1783–1809, 1964.
[17] M. Miyagi, "Bending losses in hollow and dielectric tube leaky waveguides," *Appl. Opt.*, vol. 20, no. 7, pp. 1221–1229, 1981.
[18] M. Miyagi and S. Kawakami, "Design theory of dielectric-coated circular metallic waveguides for infrared transmission," *J. Lightw. Technol.*, vol. 2, no. 2, pp. 116–126, Apr. 1984.
[19] M. Miyagi, K. Harada, and S. Kawakami, "Wave propagation and attenuation in the general class of circular hollow waveguides with uniform curvature," *IEEE Trans. Microw. Theory Techn.*, vol. 32, no. 5, pp. 513–521, May 1984.
[20] M. Miyagi and S. Karasawa, "Waveguide losses in sharply bent circular hollow waveguides," *Appl. Opt.*, vol. 29, no. 3, pp. 367–370, 1990.
[21] Y. Kato and M. Miyagi, "Modes and attenuation constants in circular hollow waveguides with small core diameters for the infrared," *IEEE Trans. Microw. Theory Techn.*, vol. 40, no. 4, pp. 679–685, Apr. 1992.
[22] Y. Matsuura *et al.*, "Loss characteristics of circular hollow waveguides for incoherent infrared light," *J. Opt. Soc. Amer. A*, vol. 6, no. 3, pp. 423–427, 1989.
[23] M. Saito *et al.*, "Bending losses of incoherent light in circular hollow waveguides," *J. Opt. Soc. Amer. A*, vol. 7, no. 11, pp. 2063–2068, 1990.
[24] Z. Du *et al.*, "Detection of methyl mercaptan with a 3393-nm distributed feedback interband cascade laser," *Appl. Phys. B*, vol. 122, no. 4, 2016, Art. no. 100-1-8.
[25] Z. Du *et al.*, "Detection of atmospheric methyl mercaptan using wavelength modulation spectroscopy with multicomponent spectral fitting," *Sensors*, vol. 17, no. 2, 2017, Art. no. 379-1-10.
[26] S. Wang *et al.*, "Measurement of atmospheric dimethyl sulfide with a distributed feedback interband cascade laser," *Sensors*, vol. 18, no. 10, 2018, Art. no. 3216-1-13.
[27] A. Naqwi and F. Durst, "Focusing of diode laser beams: A simple mathematical model," *Appl. Opt.*, vol. 29, no. 12, pp. 1780–1785, 1990.
[28] J. Yang *et al.*, "Focusing of diode laser beams: A partially coherent Lorentz model," *Proc. SPIE*, 2007, Paper 68240A, vol. 6824.
[29] P. Zhou *et al.*, "Average intensity and spreading of a Lorentz beam propagating in a turbulent atmosphere," *J. Opt.*, vol. 12, no. 1, 2010, Art. no. 015409-1-4.
[30] P. Patimisco *et al.*, "Low-loss hollow waveguide fibers for mid-infrared quantum cascade laser sensing applications," *Sensors*, vol. 13, no. 1, pp. 1329–1340, 2013.
[31] P. Patimisco *et al.*, "Low-loss coupling of quantum cascade lasers into hollow-core waveguides with single-mode output in the 3.7-7.6 μm spectral range," *Sensors*, vol. 16, no. 4, 2016, Art. no. 533-1-11.
[32] A. Sampaolo *et al.*, "Single mode operation with mid-IR hollow fibers in the range 5.1-10.5 μm," *Opt. Exp.*, vol. 23, no. 1, pp. 195–204, 2015.
[33] D. Francis *et al.*, "Quantum cascade laser light propagation through hollow silica waveguides," *Appl. Phys. B*, vol. 119, no. 1, pp. 75–86, 2015.
[34] S. Meng *et al.*, "Membership function-weighted non-linear fitting method for optical-sensing modeling and reconstruction," *Sensors*, vol. 18, no. 11, 2018, Art. no. 3762-1-14.
[35] R. Nubling *et al.*, "Launch conditions and mode coupling in hollow glass waveguides," *Opt. Eng.*, vol. 37, no. 9, pp. 2454–2458, 1998.